Sains Malaysiana 40(8)(2011): 853–864

Mapping of Faults in the Libyan Sirte Basin by Magnetic Surveys

(Pemetaan Sesar dalam Lembangan Sirte Libya dengan Survei Magnet)

SAHEEL A.S*, ABDUL RAHIM BIN SAMSUDIN & UMAR BIN HAMZAH

ABSTRACT

Magnetic surveys were carried out in Farigh area which is located in the eastern part of the Libyan Sirte basin. Interpretation of the onshore magnetic anomaly of this area, suggests that the high total magnetization may be caused by an intrusive body. Analysis of the magnetic power spectra indicates the presence of four sub-anomalies at depths of 340 m, 1400 m, and 2525 m which is probably related to the igneous rocks. The presence of igneous rock as basement at depth of 4740 m was confirmed by drilling. Assuming that all rock magnetization in the area is caused by induction in the present geomagnetic field, it strongly suggests that the causative structure has a remnant magnetization of declination (D) = –16° and inclination (I) = 23°. Based on pseudogravity data, the total horizontal derivative map shows high gradient values in NW-SW trends related to the structures in the eastern part of the Sirte basin. The 3D Euler deconvolution map derived from gravity data clearly indicates the location of igneous body in the study area as well as its tectonic trends and depth, which is estimated at 350 m to 1400 m below the surface. Depth of gravity anomalies at 1400 m to 2525 m is considered as anomalies in between shallow and deep. Anomaly at depth of approximately 4740 m below the surface is interpreted as basement rock. Geologically, the magnetic survey shows that the source of anomaly is a mafic igneous rock of Early Cretaceous age. The study also discovered a left-lateral sheared fault zone along the NW-SE of Hercynian age which was believed to be reactivated during Early Cretaceous.

Keywords: Deconvolution; fault zone; igneous bodies; magnetic survey; rock magnetization

ABSTRAK

Survei magnet telah dijalankan di kawasan Farigh yang terletak di bahagian timur lembangan Sirte di Libya. Pentafsiran yang dibuat ke atas data anomali magnet yang diperoleh di daratan mencadangkan bahawa kemagnetan jumlah yang tinggi mewakili satu jasad intrusi. Analisis data spectral kuasa menunjukkan kehadiran empat subanomali yang terletak pada kedalaman 340, 1400 dan 2525 m yang juga dikaitkan dengan batuan igneus. Kehadiran batuan igneus pada kedalaman 4740 m dibuktikan dengan data penggerudian. Jika sekiranya kesemua kemagnetan batuan dihasilkan secara aruhan medan geomagnet semasa, struktur penyebab kepada anomali magnet yang diukur mempunyai kemagnetan baki bernilai deklinasi (D) = -16° dan inklinasi (I) = 23°. Berdasarkan data pseudograviti, peta terbitan jumlah mengufuk menunjukkan kecerunan yang tinggi pada arah barat laut-tenggara yang dikaitkan dengan struktur di bahagian timur lembangan Sirte. Peta dekonvolusi Euler 3D yang dihasilkan daripada pada data graviti menunjukkan dengan jelas lokasi jasad igneus di kawasan kajian serta tren tektonik dengon kedalaman anomali yang dianggarkan terletak pada kedalaman 350 m dan 1400 m di bawah permukaan bumi. Anomali graviti pada kedalaman 1400 m dan 2525 m dianggap mewakili anomali pada kedalaman pertengahan di antara anomali cetek dan dalam. Anomali yang terletak pada kedalaman 4740 m di bawah aras permukaan ditafsirkan sebagai mewakili batuan dasar. Berdasarkan fakta geologi, survei magnet menunjukkan bahawa punca anomali merupakan batuan igneus jenis mafik yang berusia Kapur Awal. Kajian juga dapat menemukan zon sesar ricih jenis kekiri yang mempunyai tren barat laut – tenggara serta berusia Hercynian yang diaktifkan semula pada zaman Kapur Awal.

Kata kunci: Dekonvolusi; jasad igneus; kemagnetan batuan; survei magnet; zon sesar

INTRODUCTION

An aeromagnetic survey is a common type of geophysical survey carried out using a magnetometer aboard or towed behind an aircraft. The principle is similar to a magnetic survey carried out with a hand-held magnetometer, but allows much larger areas of the Earth's surface to be covered quickly for regional reconnaissance. The aircraft typically flies in a grid-like pattern with height and line spacing determining the resolution of the data (and cost of the survey per unit area). As the aircraft flies, the magnetometer records tiny variations in the intensity of the ambient magnetic field due to the temporal effects of the constantly varying solar wind and spatial variations in the Earth's magnetic field, the latter being due both to the regional magnetic field, and the local effect of magnetic minerals in the Earth's crust. A geophysicist

can use mathematical modeling to infer the shape, depth and properties of the rock bodies responsible for the anomalies. Aeromagnetic surveys are widely used to aid in the production of geological maps and are also commonly used during mineral exploration. Some mineral deposits are associated with an increase in the abundance of magnetic minerals, and occasionally the sought after commodity may itself be magnetic (e.g. iron ore deposits), but often the elucidation of the subsurface structure of the upper crust is the most valuable contribution of the aeromagnetic data.

The study area which is about 114 km^2 is located in the southern part of Concession 12 of Veba Oil field (Figure 1). This paper presents the results of processing and analysis of aeromagnetic field data over the southern part of the Farigh area (Figure 2). The principal aim of this study was to determine the depth and extent of the extrusive volcanic

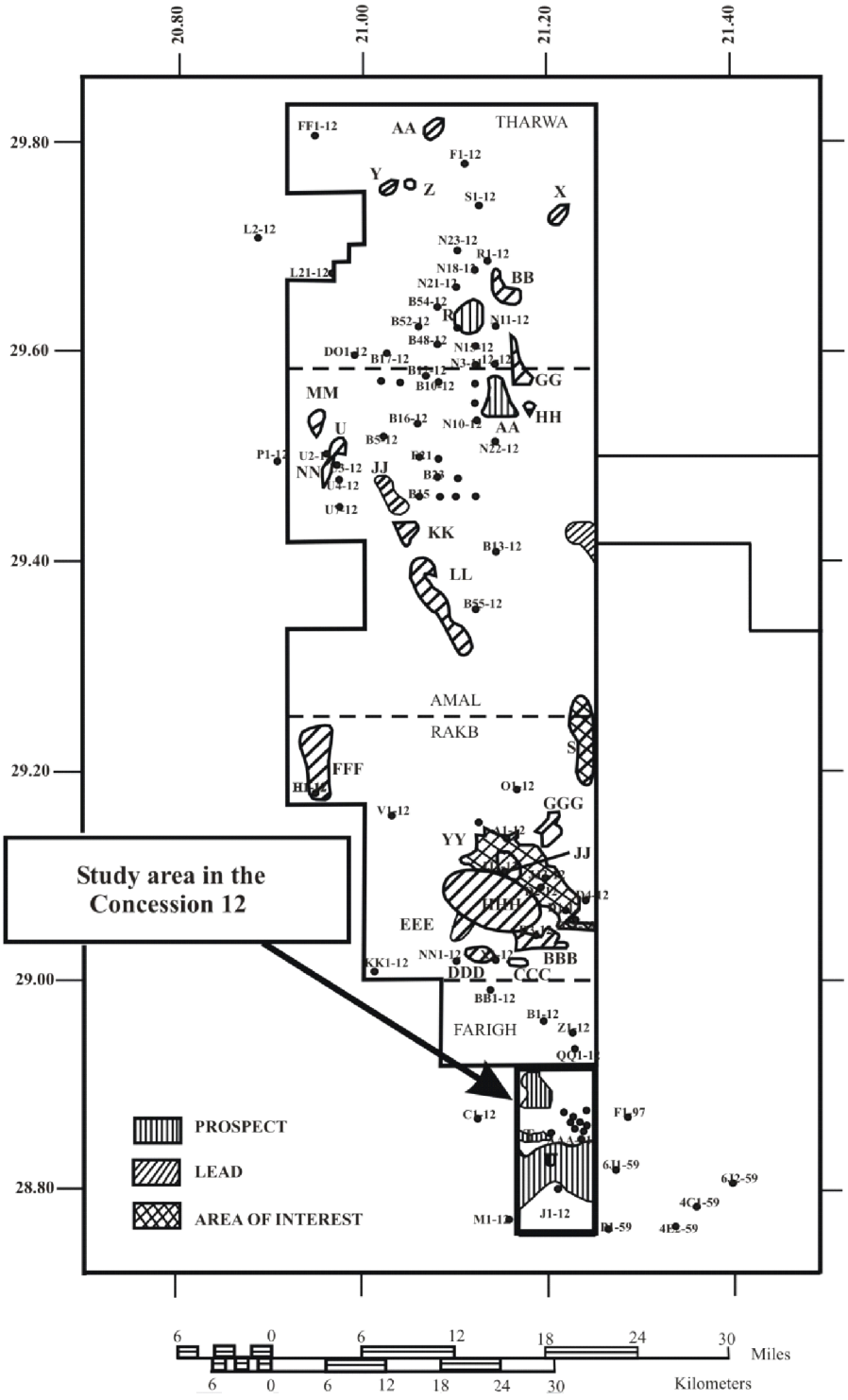

FIGURE 1. Location map of the study area (Farigh area-small box) in the concession 12 in the Sirt basin

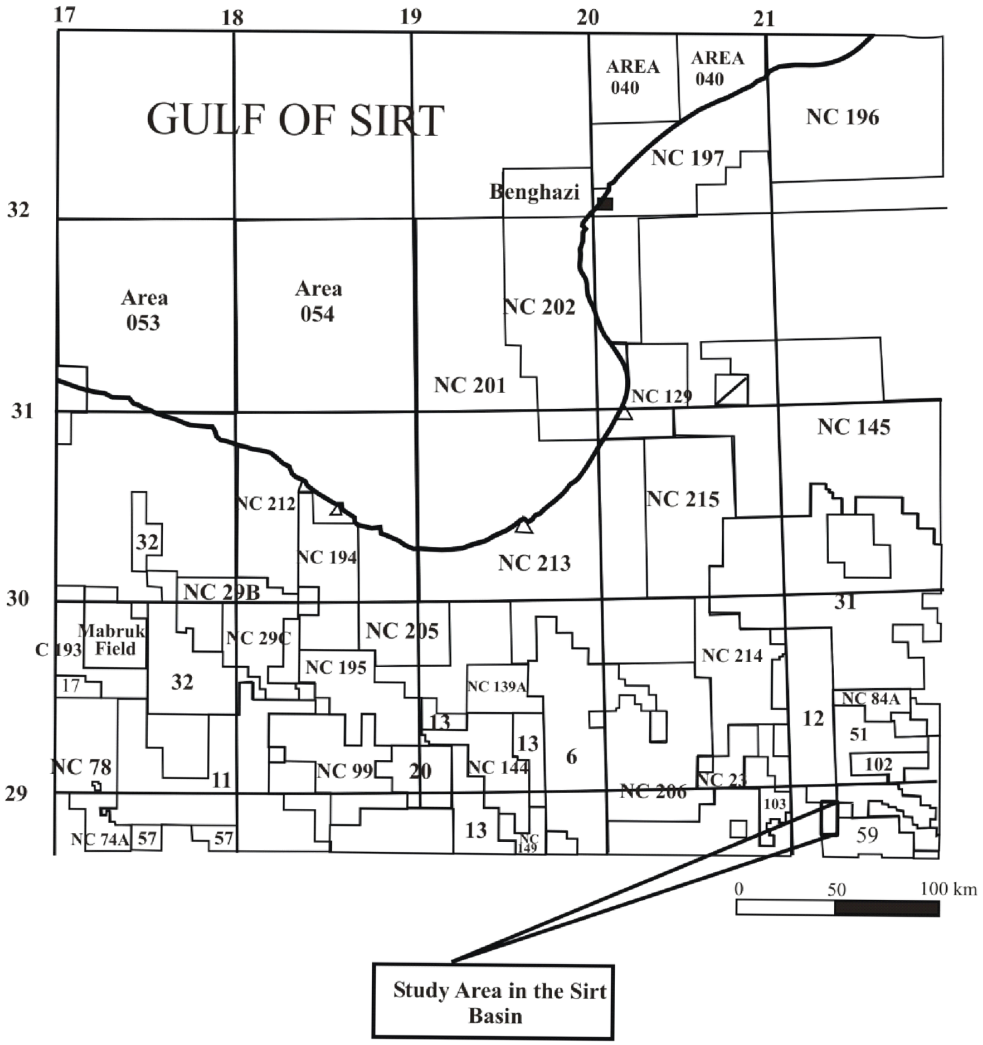

FIGURE 2. Location map of Study area (Farigh area - small box) in the Concession 12

rocks within or overlying the Nubian Sandstone. Depth of the volcanic rocks was determined by using the Energy spectrum analysis and Euler deconvolution techniques applied on magnetic data. The Horizontal Gradient technique was used to locate boundaries of magnetic data. The final results revealed new information on dominant trends of the lineaments, nature of the intrusive igneous bodies, structural features, and the age of volcanic activity.

Farigh is located near the southern boundary of Concession 12 in the eastern part of Sirte Basin. The shallow to intermediate (2 to 3 km depth) sedimentary succession of the Sirte Basin was studied through hundreds of wells data and was divided into three major sequences (Figure 3). In the central part of the Basin, the succession consists of a pre-rift (pre-Upper Cretaceous) sequence directly overlying the Precambrian basement, and overlain by the syn-rift (Upper Cretaceous-Upper Eocene) and the post-rift (Oligo-Miocene) sequences (Ahlbrandt 2001). These two sequences are marine in origin and are subdivided into various rock units, but the stratigraphic order and sedimentary characteristics of the post-rift sequence and early pre-rift sequence in the deeper parts of the Basin are poorly understood. The pre-rift (and early-rift) sequence consist of various types of continental siliciclastics deposits with some shallow marine intercalations, as well as volcanics or intrusives, ranging from Lower Paleozoic (in the case of the Gargaf Group) to Late Jurassic- Early Cretaceous (for the Nubian Sandstone and its correlatives). In the eastern part of the Sirte Basin, another sequence of siliciclastics (the Amal Group) is distinguished and entirely assigned as Triassic (Gras & Thusu 1998). These lithological characteristics are reminiscent of the Triassic “Red Beds”, and may have a relatively high magnetic susceptibility compared with typical sandstone due to a high iron oxide content. This may complicate the task of isolating the magnetic signature of intrusives or volcanics within the Nubian, particularly if they have limited lateral continuity, or occur close to the crystalline basement.

The major tectonic trends of the Arch are also believed to have controlled the post-Hercynian structure of the Sirte

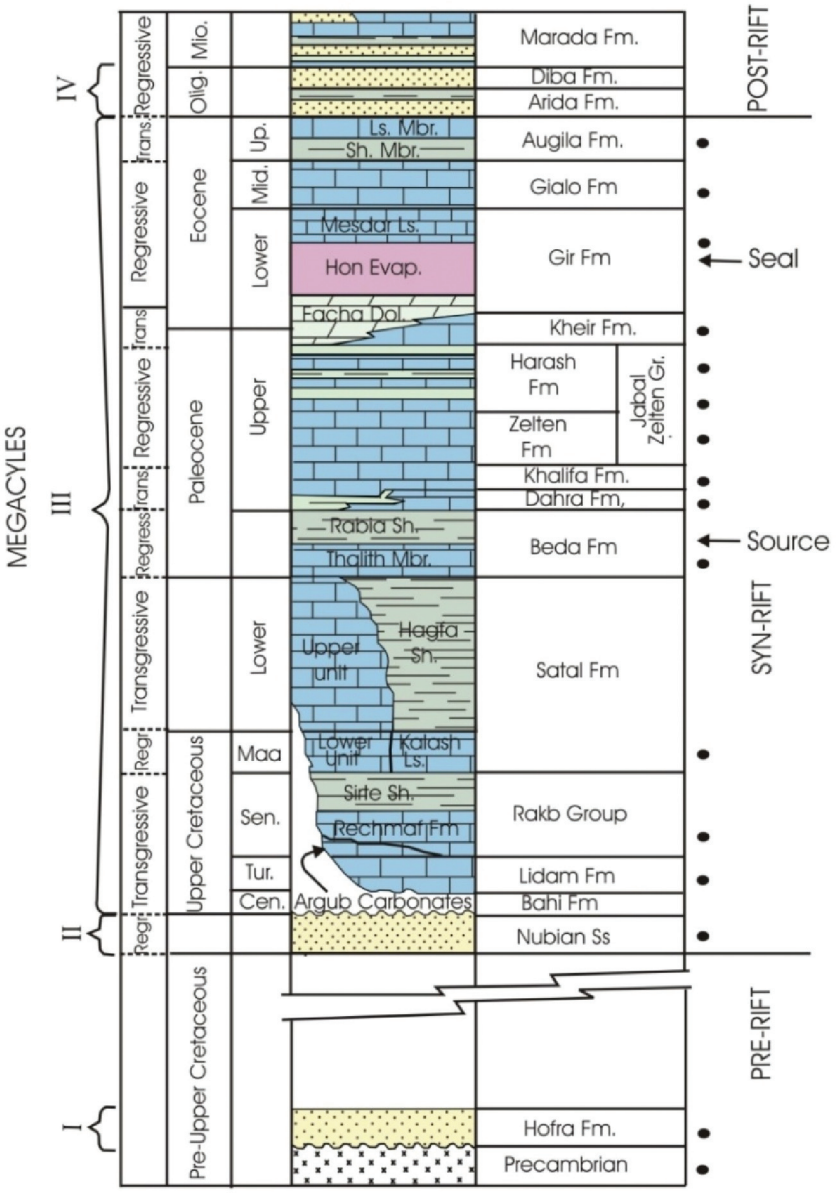

FIGURE 3. Stratigraphy section of the Sirt Basin

Basin. The Sirte Basin is widely considered to be a failed, tripartite, intra-plate rift (Ahlbrandt 2001) that started to develop in the Triassic, undergoing multiple-phased rifting, which culminated in the late Cretaceous, followed by post-rift subsidence that ceased in Oligocene. However, in the deepest, northern parts of the Basin, such as the coastal parts of the Ajdabiya Trough, subsidence continues and the thickness of the post-Hercynian sediments may reach up to 8 km (Hallet 2002). In general, compressional structures are rare, but diastrophic events (uplift, subsidence, tilting, faulting and intrusions) are prevalent (Goudarzi 1980). The northwest-southeast trend of the bounding fault (Figure 4) may be indicative of a possible earlier Hercynian faulting stage during Upper Paleozoic time.

MATERIALS AND METHODS

The aeromagnetic survey data were acquired between February 2006 and May 2006 by Worley Parsons GPX Pty. Ltd. The survey area was between 20° 45' 3.4" and 21° 20' 10.2" North, and between 28° 42' 45.3" and 29° 53' 44.6" East. The survey has a traverse spacing of 500 m (azimuth, 45° & 225°) and a tie line spacing of 2.5 km (azimuth, 135° & 315°). The nominal terrain clearance of the survey aircraft was 137 m. The magnetic data were supplied by the acquisition contractor in UTM zone 34N (WGS84) coordinates. This was the coordinate system used for all interpretation. The final High Resolution Aero Magnetic (HRAM) data was supplied in grids of 300 × 300 m^2. The inclination and declination of the centre of the survey area is 41.579° and 2.322°, respectively.

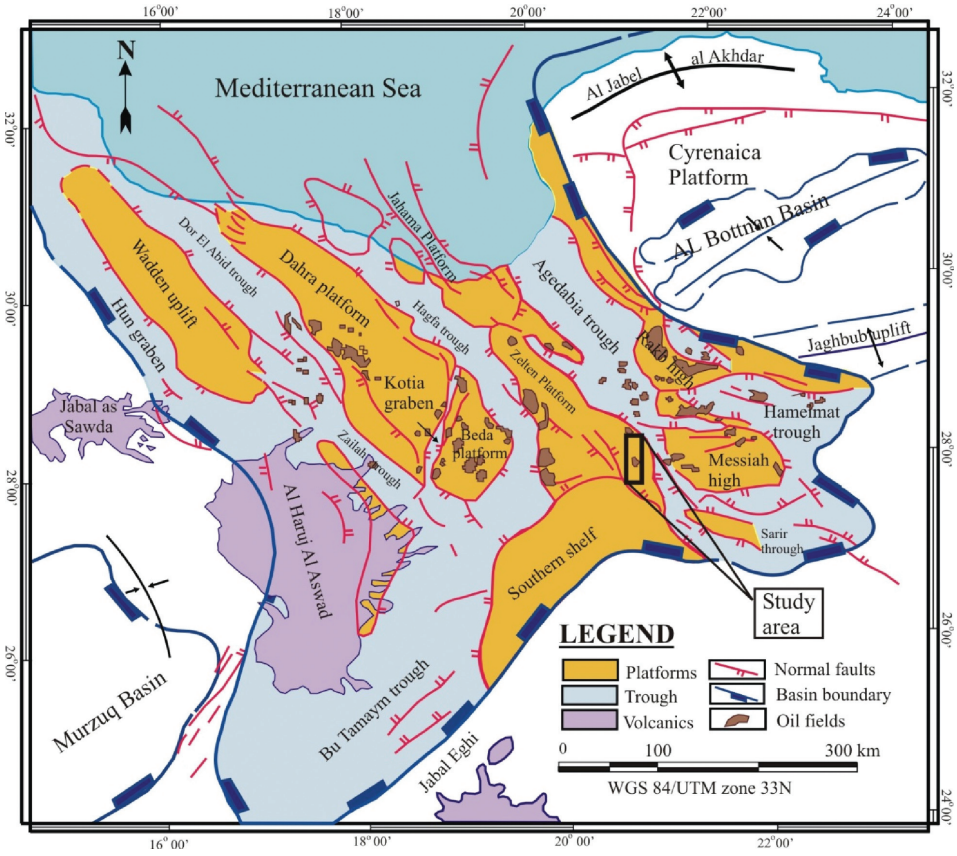

FIGURE 4. Tectonic element in the study area within the Sirt basin

The magnetic data were processed and transformed into Total Magnetic Intensity (TMI), Pesudogravity, Reduction to the Pole (RTP), calculation of power spectrum, total horizontal gradient and 3D Euler deconvolution (Figures 5, 6, 7, 8, 9 & 10). These data contain many high frequency anomalies originated from cultural sources such as power lines, pipelines and oil wells. The Geosoft software was used to transform the Poisson equation relating the gravity and magnetic field potentials expressed by $U = -(J/G\rho)\ (\partial V/\partial I)$, where U, V, I, J, ρ and G are, respectively, magnetic potential, gravitational potential, direction of magnetization, magnetization intensity, density and Gravitational constant (Geosoft 2009).

Through the use of the Geosoft software, the horizontal gradient method was applied to locate density boundaries of gravity data or susceptibility boundaries of magnetic (as Pseudogravity) data (Bilim 2007; Ma et al. 2006; Pilkington 2007). Generally, the horizontal gradient of magnetic anomaly which corresponds to a tabular body tends to overlie the edges of the body if the edges are vertical and isolated from each other (Cordell 1979; Cordell & Grauch 1985). These authors discussed a technique to estimate the location of abrupt lateral changes in magnetization or mass density of upper crest rocks. The main advantage of the horizontal gradient method is that it is least susceptible to noise in the data, because it only requires the calculations of the two first-order horizontal derivatives of the field (Phillips 1998). This method is also robust in delineating both shallow and deep sources, in comparison with the vertical gradient method, which is useful only in identifying shallower structures. The amplitude of the horizontal gradient (Cordell & Grauch 1985) is expressed as:

$$HG_g = \sqrt{\left(\frac{\partial g}{\partial x}\right)^2 + \left(\frac{\partial g}{\partial y}\right)^2}$$

where $(\partial g/\partial x)$ and $(\partial g/\partial y)$ are the horizontal derivatives of the gravity data. This method is normally applied to grid data rather than profiles. Maximum magnitudes of horizontal magnetic gradient anomaly occur above geological boundaries such as faults or steeply dipping lithological boundaries. Areas of steep lateral gradient have higher scalar amplitude values of horizontal magnetic gradient (Blakey & Simpson 1986).

The Euler deconvolution technique is used to estimate depth and location of the magnetic-gravity source anomalies. Euler deconvolution has come into wide use for automatic estimates of field source location and depth (Bournas et al. 2003; Chennouf et al. 2007; Li et al. 2008; Shepherd et al. 2006). This method was established by Thompson (1982) and has been applied essentially to real magnetic data along profiles. Reid et al. (1990) followed up a suggestion in Thompson (1982) and developed the

equivalent method, which operates on gridded magnetic data. The application of Euler deconvolution to gravity data has been carried out by several authors such as Corner and Wilsher 1989, Fairhead et al. (1994), Huang et al. (1995), Klingele et al. 1991, Marson and Klingele 1993, and Wilsher 1987.

The 3-D equation of Euler deconvolution given by Reid et al. (1990) is:

$$(x-x_o)\frac{\partial g}{\partial x}+(y-y_o)\frac{\partial g}{\partial y}+(z-z_o)\frac{\partial g}{\partial z}=\eta(\beta-g) \quad (1)$$

Equation (1) can be rewritten as:

$$x\frac{\partial g}{\partial x}+y\frac{\partial g}{\partial y}+z\frac{\partial g}{\partial z}+\eta g = x_o\frac{\partial g}{\partial x}+y_o\frac{\partial g}{\partial y}+z_o\frac{\partial g}{\partial z}+\eta\beta \quad (2)$$

where g is the magnetic or gravity anomaly detected at (x,y,z) due to a body located at (x_0,y_0,z_0). b refers to the regional field at (x,y) and h is a constant defined as "structural index" (SI), different for various geological structures. For example, in the magnetic case, SI = 3 for a sphere, SI = 2 for a horizontal cylinder and pipes, SI = 1 for sills and dykes, SI = 0.5 for thick step, SI = 0.0 for geological contacts and faults (Reid et al. 1990, 2003).

The 3D Euler deconvolution was carried as the following; horizontal (x and y directions) and first vertical grids were prepared by Geosoft routines namely GRIDHDRV and MAGMAP (Geosoft 2009). These together with the magnetic grid, were then input to EULER with the chosen structural index (SI) and window size (see below). We have assigned several structural indices values and found that an SI of 0.5 gives good clustering solutions with a window sizes. Reid et al. (1990, 2003) and Reid (2003) presented a SI = 0 is assuming a contact of infinite depth extent, SI = 0.5 is used to represent values between state for blocks or contacts of finite depth extent (maybe thickness roughly equal to depth) to top. This approximate values often give acceptable depth.

Results and Discussion

The total magnetic intensity map (TMI) of the Farigh area was calculated in an attempt to delineate its subsurface structure (Figure 5). Majority of the Farigh area is characterized by positive magnetic anomalies. This area was clearly represented as a minimum magnetic closure (42029 to 42073 nT) surrounded by higher magnetic anomalies in the north and east part of area, and the dominant trend within the study and surrounding area is NW-SE. The minimum values occurring in the north and west of the area (42030 to 42080

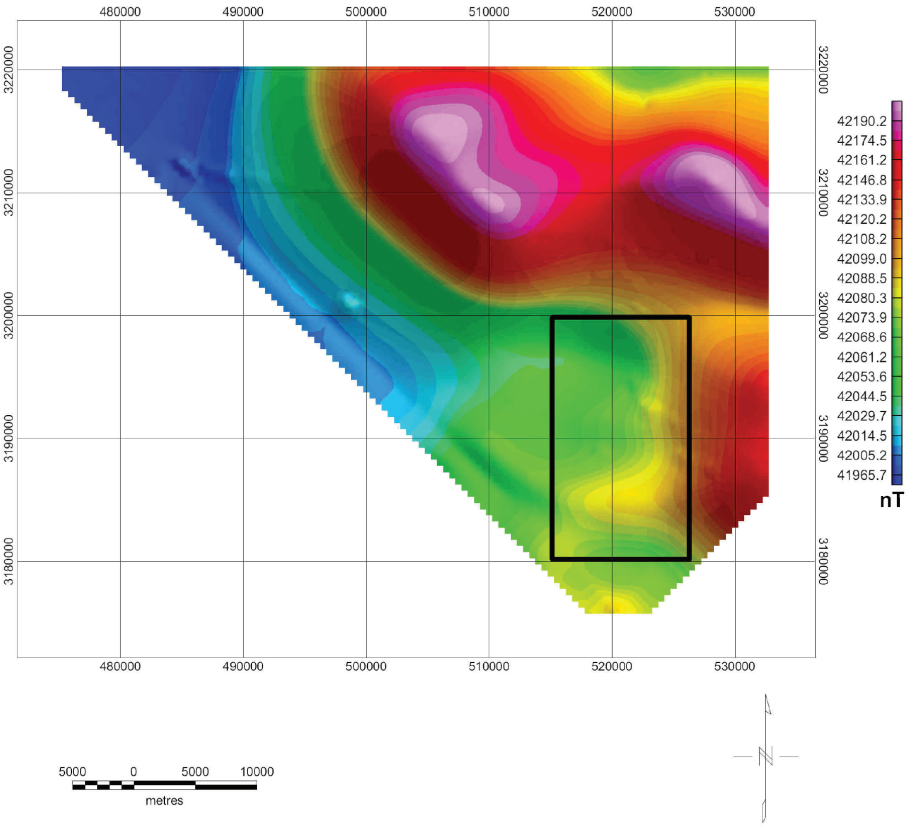

FIGURE 5. Total magnetic intensity anomaly data over study area (Farigh area, small box) and surrounding

nT) indicate thick sediments. The high positive magnetic anomalies reflected in the eastern and southern part (42088-42161 nT) indicate the presence of highly magnetic material. This can be interpreted as an anticline structure defining the existence of outcrops of Oligocene-Miocene rocks (the oldest unit in the area) on the surface. The magnetic data show the presence of intrusive igneous bodies in the southern part of the study area trending E-W in direction. Figure 6 shows that the RTP map of the study area is characterized by positive magnetic values ranging between 42086 and 42161 nT, increasing in value in the north-northeastern, south-southwestern, western and eastern parts of the study area. These areas are composed mainly of limestone, dolomite and sandstone. It can be seen that the RTP map shows a high anomaly trending NW-SE to N-S in association with some tectonic features of the area (Figure 6).

The pesudogravity field of the Farigh magnetic anomaly for induced magnetization of the present day field (I= 41.579° and D= 2.322°) shows poor correlation with the observed total magnetic intensity anomaly (Figure 5), suggesting that the causative body has a remnant magnetization. Consequently several different magnetization directions were used in the pesudogravity transformation and it was found that I= 41.579° and D= 2.322° provided a pseudogravity field in which the maximum anomaly is correlated with the maximum observed RTP anomaly (Figure 7). The orientation of the magnetization appears to be the most realistic estimate of the total magnetization vector orientation. In the tectonic section, this direction of magnetization is Early Cretaceous (160-170 Ma) in age. During this time the second phase of mainly NW-SE oriented rifting started within the central part of the Basin in the late Aptian, migrating towards the north-northwest (Guiraud & Bosworth 1997).

The power spectrum of the reduced to the pole magnetic grid, which represents the magnitude of various frequency components of a 2D image, was computed by Fourier transform and seems in agreement with the location of the main source at the origin of the anomaly (Geosoft 2009). The spectrum shows 4 very clear anomalies at depths below aircraft of 340 m, 1400 m, 2525 m and 4740 m. The shallowest slice (Figure 8(a)) at depth 341 m appears to correspond very strongly to surface features interpreted as pipeline and wells. These data were derived from flying height of 400 m above the ground. The deepest slice at depth of 4750 m produced anomaly (Figure 8(b)) which corresponds to basement rock. The intermediate depths in the power spectrum may represent the volcanic rocks (1400 m and 2525 m, Figure 8(a) and (b)). However, Figure 9 shows the horizontal-gradient map of the study area. The magnetic field was transformed into a pseudogravity field using I= 41.579° and D= 2.322°. From the pseudogravity field, the magnitude of horizontal gradient was calculated by using Geosoft software. High gradient values indicated

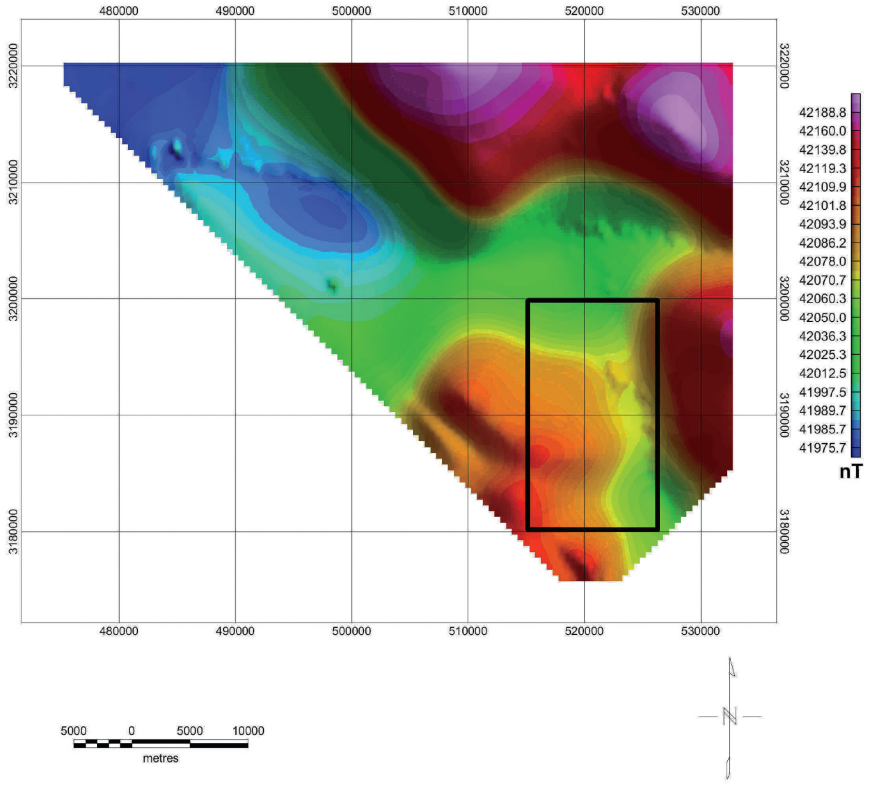

FIGURE 6. Reduction to the Pole of magnetic data over study area (Farigh area, small box) and surrounding

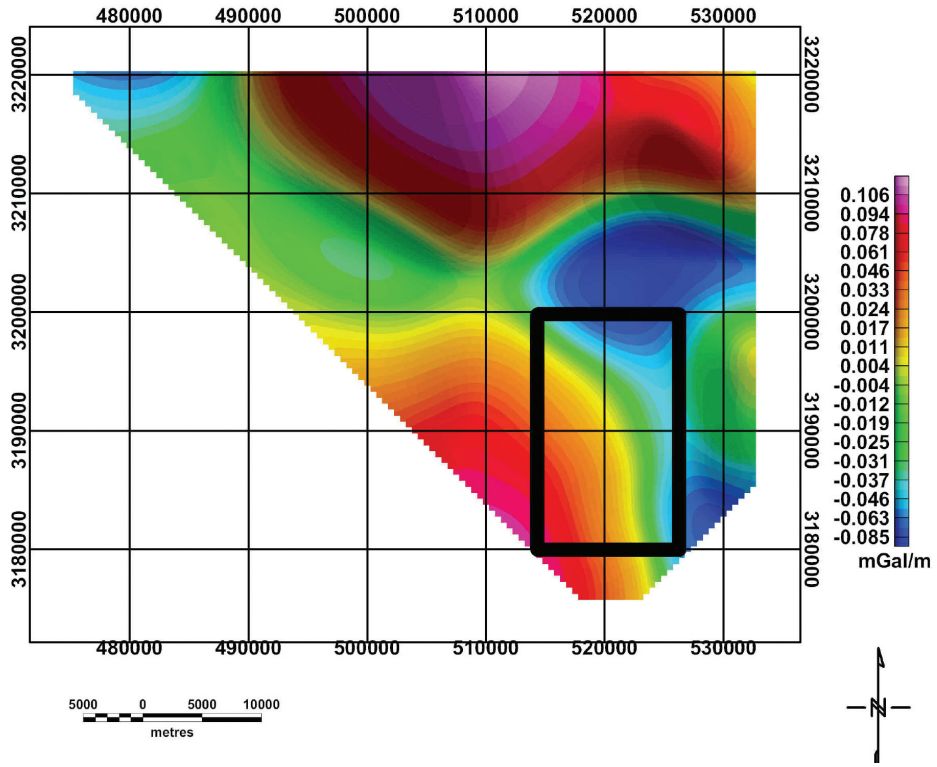

FIGURE 7. Pseudogravity anomaly map over study area (Farigh area, small box) and surrounding

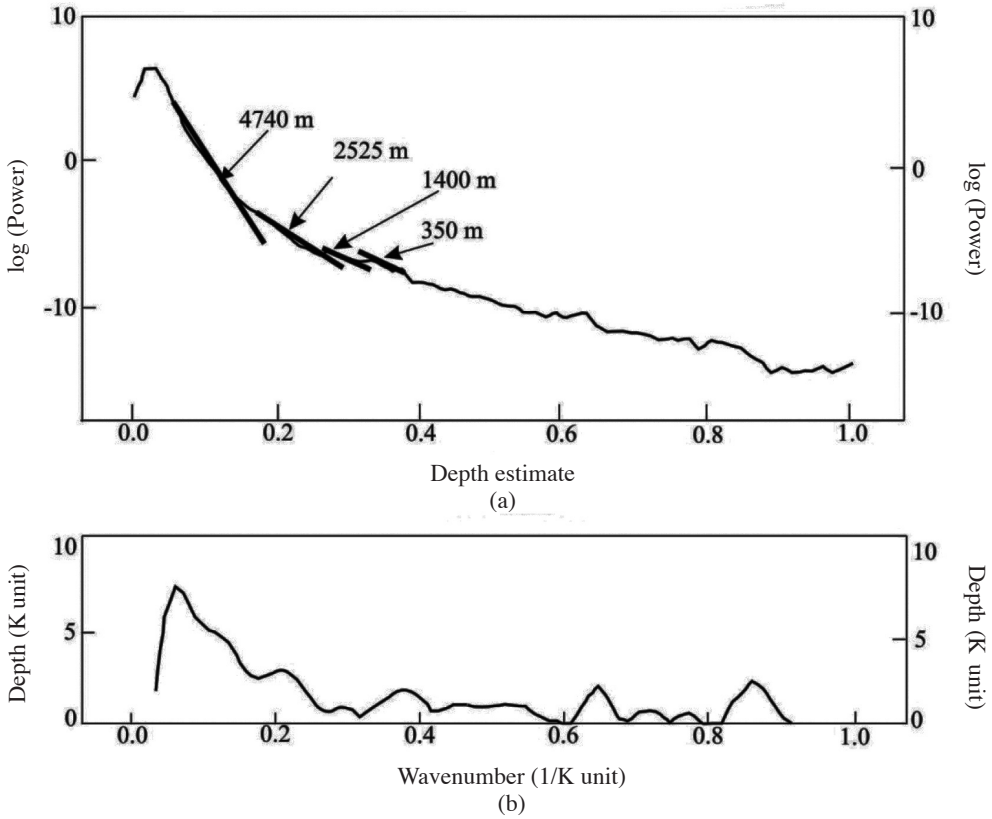

FIGURE 8. Power spectrum result of the study area (Farigh area) (a) log Power versus depth and (b) depth versus wavenumber

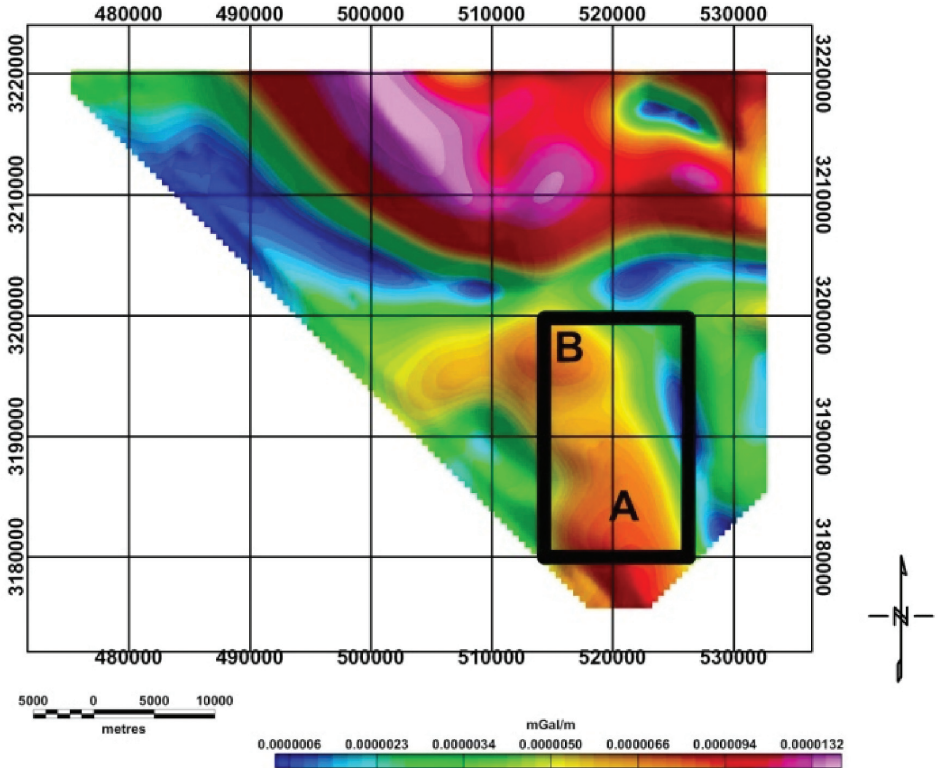

FIGURE 9. Total horizontal derivative map of Pseudogravity (after transfer Total Magnetic Intensity) in the Farigh area (small box) and surrounding

as A and B (Figure 9) were observed at locations that may be interpreted as the igneous bodies of the study area. The directions of the bodies are estimated in NW-SE direction.

In this area of study and in the surrounding area, the Euler method was applied to measure the magnetic data using a moving window size of 10 (40 km × 40 km), and an SI of 0.5 which showed good "focusing" of solution positions (Figure 10). Results of the Euler deconvolution of re-gidding magnetic data (400 m, high resolution) in the study area (Farigh area, small box) using a moving windows size of 10 (4 km × 4 km), and an SI = 0.5 are shown in Figure 11. The interpretation of Euler solutions indicates that the NW-SE anomalies were truncated by NE-SW trends and characterized the whole structural setting or faults of the Farigh area. The depth of fault contacts ranges from power spectrum applied to Euler depth are 350, 2525, 1400 and 4740 m, respectively. These contacts were interpreted as contacts plotted and statistically analyzed (Figure 11). The depth levels of 1400 and 2525 m (Figure 11) are chosen to cover structural boundaries in the top of igneous bodies (especially Nubian sandstone) indicates that the depth from borehole (J1-12) penetrated the igneous bodies are matched with the results of Euler deconvolution in the study area.

The body which caused the anomaly in the study area originated from a depth similar to the depth of igneous rocks determined in boreholes penetrated in the Farigh area. The J1-12 borehole data indicate that these igneous rocks do not contribute significantly to the magnetic anomaly because of either their low magnetization intensity or their alteration. The high amplitudes of the magnetic and RTP anomalies indicate that they are caused by a highly-magnetized igneous body that probably comprises mafic igneous rocks, as these are the most common ferromagnetic rocks with high magnetization. There is a lot of interference originating from shallow surface features in the power spectrum. There are indications of possible occurrence of volcanic rocks at depths of 1400 m and 2525 m below aircraft, however it is not possible to map their spatial distribution. The basement is at depth of 4740 m below aircraft. It is true that during Cretaceous, the geomagnetic field of African continent coincided with the present-day direction. If there were remanence of this age, it would be impossible to detect them in the airborne data, because it would probably be similar to the induced magnetization. It is therefore invalid to conclude that there is Cretaceous remanence magnetization. The magnetic anomaly shows a NW-SE trend which is a common tectonic element in the Sirt basin such as the southeastern Sirt basin fault system and the East-west Hameimat fault zones. This trend is formed during Hercynian events. The pseudogravity anomaly in the southwestern termination of the Farigh area is the only obvious representative of the NW-SE Sirt trend. This again emphasises the secondary nature of these fractures, derived in response to WNW-ESE faulting which itself was probably influenced by pre-existing magnetic basement terrain boundaries.

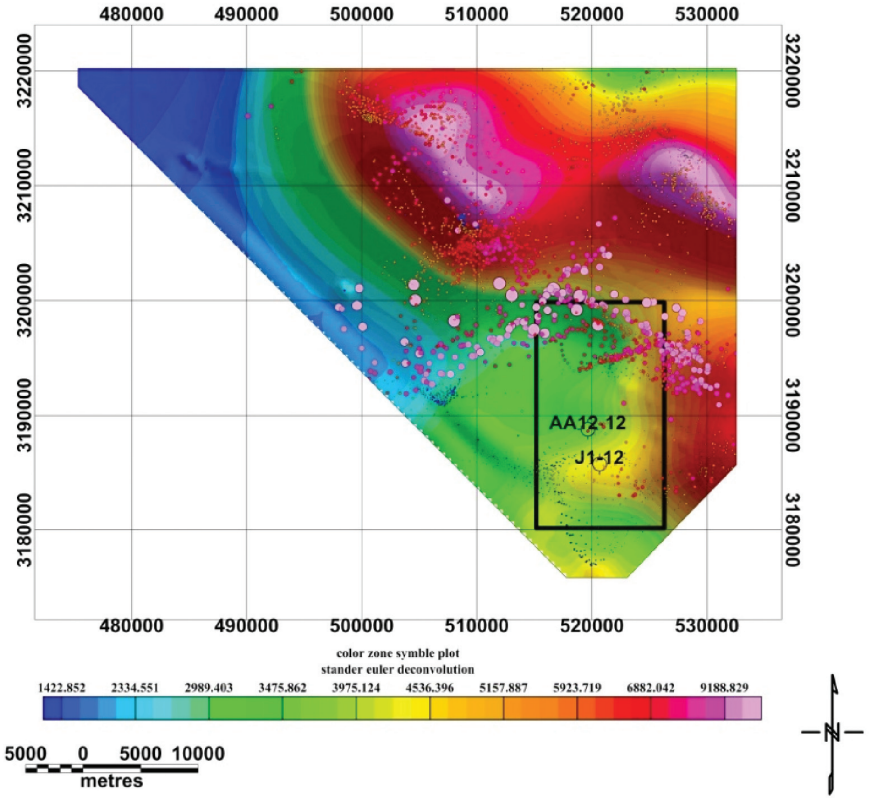

FIGURE 10. 3D Euler deconvolution for magnetic intensity anomaly in the study area (Farigh area, small box) and surrounding, using grid cell size 4 km. SI = 0.5, W = 10 (40 km × 40 km)

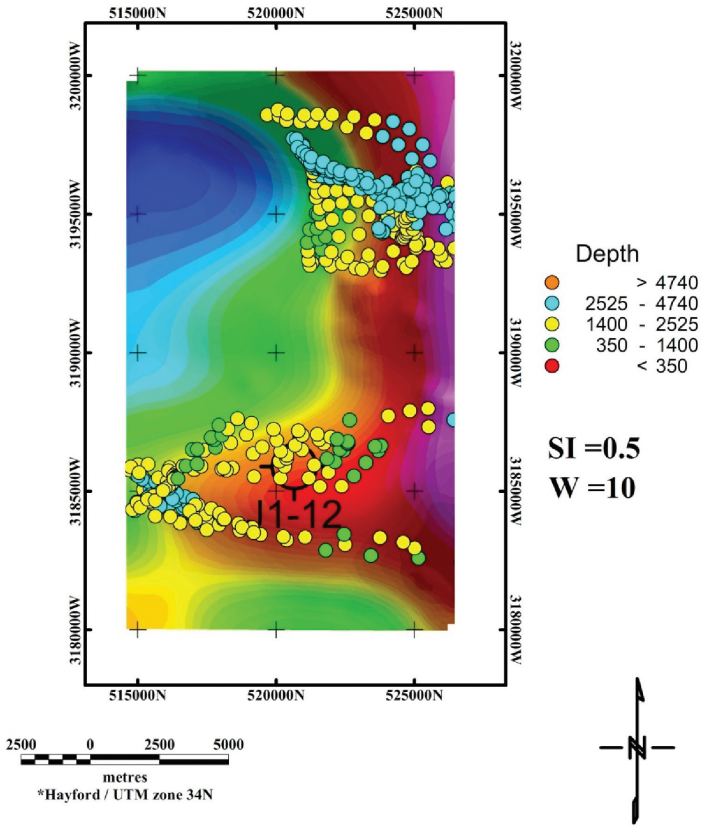

FIGURE 11. 3D Euler deconvolution for magnetic intensity anomaly over Farigh area, using grid cell size 400 m SI = 0.5,W = 10 (4 km × 4 km)

CONCLUSION

Total magnetic derivative results compare very well with the 3D Euler Deconvolution and tectonic elements in the study area. High magnetic gradient values delineate NW-SE and E-W fault trends which mark the faulted eastern and southern part of Sirte basin, respectively. Estimated depth of igneous body in the study area from 3D Euler deconvolution applied to the total magnetic intensity data using structural index SI = 0.5 and window size W=10 is from 350 m to 1400 m represents solutions in the shallow parts of study area. Depth of 1400 m to 2525 m are critically indicative of intermediate depth. Deeper solution at depth of 4740 m below the surface is interpreted as basement rocks.

ACKNOWLEDGEMENTS

We thank the National Oil Corporation of Libya and the Libyan Petroleum Institute for their permission to publish the present data. Thanks are also due to Dr A.B. Reid for his advice concerning the application of Euler deconvolution.

REFERENCES

Ahlbrandt, T.S. 2001. The Sirte Basin Province of Libya: Sirte-Zelten Total Petroleum System. *U.S. Geological Survey Bulletin* 2202-F (Version 1.0)

Bilim, F. 2007. Investigations into the tectonic lineaments and thermal structure of Kutahya-Denizli region, western Anatolia, from using aeromagnetic, gravity and seismological data. *Physics of the Earth and Planetary Interiors* 165(3-4): 135-146.

Blakely, R.J. & Simpson, R.W. 1986. Locating edges of source bodies from magnetic and gravity anomalies. *Geophysics* 51(7): 1494-1498.

Bournas, N., Galdeano, A., Hamoudi, M. & Baker, H. 2003. Interpretation of the aeromagnetic map of Eastern Hoggar (Algeria) using the Euler deconvolution, analytic signal and local wavenumber methods. *Journal of African Earth Sciences* 37(3-4): 191-205.

Chennouf, T., Khattach, D., Milhi, A., Andrieux, P. & Keating, P. 2007. Major structural trends in northeastern Morocco: The contribution of gravimetry. *Comptes Rendus – Geoscience* 339: 383-395.

Cordell, L. & Grauch, V.J.S. 1985. Mapping basement magnetization zones from aeromagnetic data in the San Juan Basin, New Mexico. In Hinze, W. J., Ed., *The utility of regional gravity and magnetic anomaly maps:* Society of Exploration Geophysicists: 181-197.

Cordell, L. 1979. Gravimetric expression of graben faulting in Santa Fe Country and the Espanola Basin, New Mexico, *Guidebook to the 30th Field Conference, Santa Fe Country, New Mexico Geological Society (Ed)*, New Mexico Geological Society, Socorro: 59-64.

Corner, B. & Wilsher, W.A. 1989. Structure of the Witwatersrand basin derived from interpretation of the aeromagnetic and gravity data. In Garland, G. D., Ed., *Proceedings of Exploration '87, Third Decennial International Conference on Geophysical and Geochemical Exploration for Minerals and Groundwater: Ontario Geological Survey, Special* 3: 532-546.

El-Hawat, A.S., Missallati, A.A, Bezan, A.M. & Taleb, T.M. 1996. The Nubian Sandstone in Sirte Basin and its Correlatives. In: Salem, AJ, El-Hawat, AS and AM Sbeta (Eds), *The Geology of Sirt Basin*. Amsterdam: Elsevier, p. 3-30.

Fairhead, J.D., Bennet, K.J., Gordon, R.H. & Huang, D. 1994. Euler: Beyond the Black Box. *64th Annual International Meeting, Society of Exploration Geophysicists, Expanded Abstracts,* pp. 422-424.

Geosoft Reference Manual 2009. *Software for Earth Sciences Geosoft INC*., Toronto, Cana.

Goudarzi, G.H. 1980. Structure- Libya. In: Salem, MJ and Buserwil, MI (editors). *The Geology of Libya*. 3: 879-892. London, UK: Academic Press.

Gras, R. & Thusu, B. 1998. Trap architecture of the Early Cretaceous Sarir Sandstone in the eastern Sirt Basin. In: Macgreor, DS, Moody, RTJ and DD Clark-Lowes (eds), Petroleum Geology of North Africa. *Geological Society, London, Special Publication* No:132: 317-334.

Guiraud, R. & Bosworth, W. 1997. Senonian basin inversion and rejuvenation of rifting in Africa and Arabia: synthesis and implications for plate scales tectonics. *Tectonophysics* 282: 39-82.

Hallet, D. 2002. *Petroleum Geology of Libya*. 487 pp, Elsevier, Amsterdam.

Huang, D., Gubbins, D., Clark, R.A. & Whaler, K.A. 1995. Combined study of Euler's homogeneity equation for gravity and magnetic field. *57th Conference and Technical Exhibition EAGE, Glasgow, Extended Abstracts*, P144.

Klitzsch, E.H. & Squyres, C.H. 1990. Paleozoic and Mesozoic geological history ofnortheastern Africa based upon new interpretation of Nubian Strata. *The AAPG Bull*. 74: 1203-1211.

Klitzsch, E. 1971. The structural development of part of north Africa since Cambrian time. In: Gray, C (editor), *First Symposium on the Geology of Libya*. Faculty of Science,University of Libya, pp. 253-262, Tripoli.

Klingele, E.E., Marson I., & Kahle, H.G. 1991. Automatic interpretation of gravity gradiometric data in two dimensions: vertical gradient. *Geophysical Prospecting* 39: 407-434.

Tawadros, E, Rasul, S.M. & Elzaroug, E. 2001. Petrography and palynology of quartzite in the Sirte Basin, central Libya. *Jour. African Earth Sciences* 32: 373-390.

Li, C.-F., Zhou, Z., Hao, H., Chen, H., Wang, J., Chen, B. & Wu, J. 2008. Late Mesozoic tectonic structure and evolution along the present-day northeastern South China Sea continental margin. *Journal of Asian Earth Sciences* 31(4-6): 546-561.

Ma, Z.-J., Gao, X.-L. & Song, Z.-F. 2006. Analysis and tectonic interpretation to the horizontal-gradient map calculated from Bouguer gravity data in the China mainland. *Chinese Journal of Geophysics (Acta Geophysica Sinica)* 49(1): 106-114.

Marson, I., & Klingele, E.E. 1993. Advantages of using the vertical gradient of gravity for 3-D interpretation. *Geophysics* 58: 1588-1595.

Phillips, J.D. 1998. Processing and interpretation of aeromagnetic data for the Santa Cruz Basin-Patahonia Mountains area, South-Central Arizona. *U.S. Geological Survey Open-File Report* 02-98.

Pilkington, M. 2007. Locating geologic contacts with magnitude transforms of magnetic data. *Journal of Applied Geophysics* 63(2): 80-89.

Reid, A.B. 2003. Short note: Euler magnetic structural index of a thin-bed fault. *Geophysics* 68: 1255-1256.

Reid, A.B., Allsop, J.M., Granser, H., Millet, A.J. & Somerton, I.W. 1990. Magnetic interpretation in three dimensions using Euler Deconvolution. *Geophysics* 55: 80-91.

Reid, A.B., FitzGerald D. & McInerney P. 2003. Euler Deconvolution of gravity data. *Society of Exploration Geophysicists (SEG), Annual Meeting,* 2003, pp. 580-583.

Robertson, 1970. Geological study in the concession 12. Unpblished report.

Shepherd, T., Bamber, J.L. & Ferraccioli, F. 2006. Subglacial geology in Coats Land, East Antarctica, revealed by airborne magnetics and radar sounding. *Earth and Planetar Science Letters* 244(1-2): 323-335.

Thompson, D.T. 1982. EULDPH – A new technique for making computer-assisted depth estimates from magnetic data. *Geophysics* 47: 31-37.

Van der Meer, F. & Cloetingh, C. 1993. Intraplate stresses and subsidence history of the Sirte Basin (Libya). *Tectonophysics* v. 226: 37-58.

Wilsher, W.A. 1987. A structural interpretation of the Witwatersrand basin through the application of the automated depth algorithms to both gravity and aeromagnetic data. Thesis (MSc). University of Witwatersrand. (Unpublished)

A.S. Saheel*
Libyan Petroleum Institute-Tripoli-Libya

Abdul Rahim Bin Samsudin & Umar Bin Hamzah
School of Environment and Natural Resource Sciences
Faculty of Science and Technology
Universiti Kebangsaan Malaysia
43600 Bangi, Selangor
Malaysia

*Corresponding author; email: ahmedsaheel423@yahoo.com

Received: 8 February 2010
Accepted: 23 September 2010